Modeling of Wetting: A Study of Nanowetting at Rough and Heterogeneous Surfaces

Mathias Lundgren, Neil L. Allan, and Terence Cosgrove*

School of Chemistry, University of Bristol, Cantock's Close, Bristol BS8 1TS, U.K.

Received March 16, 2006. In Final Form: September 20, 2006

Molecular dynamics simulations were performed to study the behavior of nanoscale water droplets at solid surfaces. Simulations of droplets on heterogeneous patterned surfaces show that the relative sizes of the domains and the droplets play an important role as do the interactions between the solid and the liquid, particularly when the domain width is comparable to the droplet radius. For pillar surfaces, a transition is observed between the Wenzel and the Cassie and Baxter regimes with increasing pillar height. The effects of pillar width and the gap between the pillars were also examined. The simulations show clearly the importance of the detailed topography and composition of the solid surface.

1. Introduction

The wetting of solid surfaces by liquids is of fundamental importance in areas of everyday life ranging from biology to industrial applications. A striking example is the remarkable nonwetting properties of the lotus plant leaf.[1,2] When a raindrop hits the leaf, it is completely repelled from the surface and rolls off the leaf rather than sliding. The rolling is due to the microscopic structure of the leaf; the process keeps the plant dry during heavy showers, and the rolling droplets remove particles of dirt. The surface contact of a water droplet on a lotus leaf is only ∼2 to 3%.

Exciting results have recently been reported by Feng et al.[3] for a droplet spreading on a ZnO nanorod surface. The surface showed *both* superhydrophobic and superhydrophilic properties. The wettability is changed dramatically by exposing the surface to ultraviolet radiation, and the results appear to be due to a combination of the nanostructure and the photosensitivity of the surface.

The molecular processes and the relationships between wetting and surface structure that underlie the different phenomena observed are thus of particular interest.[4] Molecular dynamics (MD) simulations have been used by several authors[5−16] to study the spreading of small-scale droplets. Many of these have been restricted to the use of short-range Lennard-Jones potentials,[6,10−15] but only a few simulations including Coulombic forces[16,17] have been reported. Such long-range interactions can play important roles in determining the orientations of molecules at the interfaces.

In previous work, we have presented results of MD simulations of wetting of a graphite surface by water/ethanol droplets.[18] Even though the droplet contained only approximately 1000 molecules, the calculated contact angles were in good agreement with those obtained experimentally for much larger macroscopic droplets. Time-averaged structural analyses showed that the ethanol molecules formed a monolayer on top of the surface; there is competitive adsorption between the solid−liquid and the liquid−vapor interfaces.

In this article, we extend our simulation studies to more complex surfaces and structures.[19] We start with heterogeneous surfaces. For such an interface, the Cassie equation relates the observed actual contact angle to the fractional areas of the different components of the surface. If the solid surface is composed of two materials, then the contact angle is assumed to be a function of the two separate contact angles on the pure substrates such that[20]

$$\cos\theta = f_A \cos\theta_A + f_B \cos\theta_B \quad (1)$$

f_A and f_B are the fractional areas of the two compounds, and θ_A and θ_B are the contact angles on smooth heterogeneous surfaces of pure A and pure B, respectively. Theoretical work[21] has suggested that the distribution of the heterogeneous islands on the surface can lead to the breakdown of the Cassie equation, especially for nanodroplets.[22] A water droplet with a radius much smaller than the width of the domains will spread over the hydrophilic part, A, taking up a contact angle close to θ_A. When the volume of the droplet is larger, it spreads on top of the surface until it reaches the boundary of the hydrophobic part. The droplet may stay on the hydrophilic domain, but the contact angle is

* Corresponding author. E-mail: terence.cosgrove@bristol.ac.uk.

(1) Barthlott, W.; Neinhuis, C. *Planta* **1997**, *202*, 1.
(2) Neinhuis, C.; Barthlott, W. *Ann. Bot.* **1997**, *79*, 667.
(3) Feng, X.; Feng, L.; Jin, M.; Zhai, J.; Jiang, L.; Zhu, D. *J. Chem. Soc.* **2004**, *126*, 62.
(4) Fan, J. G.; Tang, X. J.; Zhao, Y.-P. *Nanotechnology* **2004**, *15*, 501.
(5) Hautman, J.; Klein, M. L. *Phys. Rev. Lett.* **1991**, *67*, 1763.
(6) Blake, T. D.; Clarke, A.; DeConinck, J.; deRuijter, M. J. *Langmuir* **1997**, *13*, 2164.
(7) de Ruijter, M. J.; De Coninck, J.; Blake, T. D.; Clarke, A.; Rankin, A. *Langmuir* **1997**, *13*, 7293.
(8) Fan, C. F.; Cagin, T. *J. Chem. Phys.* **1995**, *103*, 9053.
(9) Bresme, F.; Quirke, N. *Phys. Rev. Lett.* **1998**, *80*, 3791.
(10) De Coninck, J.; Voue, M. *Interface Sci.* **1997**, *5*, 141.
(11) Dortona, U.; DeConinck, J.; Koplik, J.; Banavar, J. R. *Phys. Rev. E* **1996**, *53*, 562.
(12) De Coninck, J. *Colloids Surf., A* **1996**, *114*, 155.
(13) Cazabat, A. M.; Valignat, M. P.; Villette, S.; DeConinck, J.; Louche, F. *Langmuir* **1997**, *13*, 4754.
(14) Gentner, F.; Ogonowski, G.; De Coninck, J. *Langmuir* **2003**, *19*, 3996.
(15) Voue, M.; Rovillard, S.; De Coninck, J.; Valignat, M. P.; Cazabat, A. M. *Langmuir* **2000**, *16*, 1428.
(16) Werder, T.; Walther, J. H.; Jaffe, R. L.; Halicioglu, T.; Koumoutsakos, P. *J. Phys. Chem. B* **2003**, *107*, 1345.
(17) Hautman, J.; Bareman, J. P.; Mar, W.; Klein, M. L. *J. Chem. Soc., Faraday Trans.* **1991**, *87*, 2031.
(18) Lundgren, M.; Allan, N. L.; Cosgrove, T.; George, N. *Langmuir* **2002**, *18*, 10462.
(19) Lundgren, M.; Allan, N. L.; Cosgrove, T.; George, N. *Langmuir* **2003**, *19*, 7127.
(20) Cassie, A. B. D. *Discuss Faraday Soc.* **1948**, *3*, 11.
(21) Padday, J. F., Ed. *Wetting, Spreading and Adhesion*; Academic Press: New York, 1978.
(22) Brandon, S.; Haimovich, N.; Yeger, E.; Marmur, A. *J. Colloid Interface Sci.* **2003**, *263*, 237.

10.1021/la060712o CCC: $37.00
Published on Web 11/23/2006

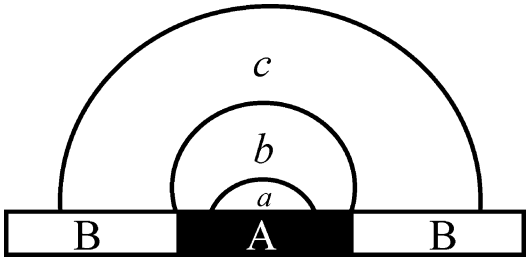

Figure 1. Schematic picture of the equilibrium position of the droplet on a solid surface composed of compounds A and B. For the small droplet a, compound A is partially wetted, and droplet b wets the A surface completely. In contrast, the large drop wets both surface types.

higher as a result of the volume increase. Further increase in volume forces the contact line to move across the boundary to the hydrophobic area. The different possible outcomes are shown schematically in Figure 1. Hence, although eq 1 predicts a single value of the contact angle, multiple contact angles may be observed experimentally[21] as a result of the existence of multiple metastable states corresponding to local minima. The Cassie approximation should become more accurate as the size of the drop exceeds that of the heterogeneities on the surface;[22,23] the validity thus depends on the volume of the droplet relative to the sizes of the heterogeneous domains. Similar trends are seen when the domain areas are changed and the drop volume is kept constant.

Turning to rough surfaces, it is crucial to the wetting properties as to whether the liquid molecules penetrate the hollows of the rough surface. If the liquid does penetrate and the surface is dry ahead of the contact line, then the equation of Wenzel[24] predicts that the contact angle for the perfectly smooth surface, θ_0, is multiplied by a roughness factor r, and

$$\cos\theta = r\cos\theta_0 \tag{2}$$

r is the ratio of the areas of the rough and the corresponding smooth surface. The hydrophobicity of the rough surface is assumed to be the same as that of the smooth. The Wenzel equation predicts enhanced wetting with increasing roughness when $\theta_0 < 90°$ and decreased wetting when $\theta_0 > 90°$.

If the liquid is excluded from the hollows of the surface, then the droplet may be in contact with only the "upper" part of the surface and the contact angle θ tends to 180°. Wenzel's approximation is then no longer valid, and an alternative is to treat the roughness as a heterogeneity and use the Cassie equation.[20] If the second material B is air, then the corresponding contact angle is 180°, and eq 1 becomes the Cassie and Baxter equation[25]

$$\cos\theta = f(\cos\theta_0 + 1) - 1 \tag{3}$$

where $f = f_A$ and $\theta_0 = \theta_A$.

The superhydrophobic surfaces of particular current interest are composed of posts of various dimensions and shapes.[26] To design a surface to give rise to a high contact angle, these posts must be close together and sufficiently hydrophobic to prevent the intrusion of liquid molecules between the gaps of the posts, as shown in Figure 2. The base of the droplet thus involves both the liquid−solid and liquid−air interfaces. Cassie and Baxter's analysis does not take into account the structure of the three-phase contact line, which will vary with surface geometry. Rough surfaces with the same value of f but different topographies may have different locations of the contact line and contact angles. However, the Cassie and Baxter equation predicts the same equilibrium contact angle for all of these surfaces.

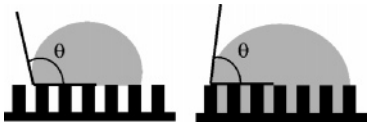

Figure 2. Schematic picture of a droplet in the Cassie regime (left frame) and Wenzel regime (right frame) surface. For pillar surfaces throughout this article, the contact angle, θ, is defined as that at the top of the pillars.

There have been several studies of wetting of such systems using macroscopic interfacial thermodynamics.[27−44] Such methods have, for example, examined the relative stability of droplets in the Cassie and Wenzel regimes, possible multiple free-energy minima for droplets and hysteresis associated with the contact angle. On the mesoscopic scale, lattice Boltzmann techniques have been used to investigate the dynamics of the transition between the Wenzel and Cassie regimes, including gravitational effects.[45]

In this article, we consider behavior on a much smaller molecular length scale. We have previously reported a preliminary molecular-scale simulation of water droplets at pillar surfaces composed of sheets of carbon atoms and examined the variation of the contact angle with the height of the pillars.[19] An objective of the current article is to extend these studies to a much wider range of solid surfaces, including the effects of surface topography, roughness, and heterogeneity, and compare the results with those predicted by the widely used empirical models (eqs 1 and 3). Our work complements very recent application to this type of problem of lattice gas models solved using a mean-field approximation on short length scales.[46,47]

Thus, in this article, results of MD simulations of water droplets at a variety of well-defined surface structures are presented. In section 2, we discuss the simulation methods and the computational details. Results for wetting at planar heterogeneous surfaces are presented in section 3, considering square and stripe domains of different sizes (section 3.1) and the effects of altering the surface composition (section 3.2). Section 4 turns to pillar surfaces, varying the pillar height (section 4.1), pillar width

(23) Brandon, S.; Wachs, A.; Marmur, A. *J. Colloid Interface Sci.* **1997**, *191*, 110.
(24) Wenzel, R. N. *Ind. Eng. Chem.* **1936**, *28*, 988.
(25) Cassie, A. B. D.; Baxter, S. *Trans. Faraday Soc.* **1944**, *40*, 546.
(26) Oner, D.; McCarthy, T. J. *Langmuir* **2000**, *16*, 7777.
(27) Otten, A.; Herminghaus, S. *Langmuir* **2004**, *20*, 2405.
(28) Patankar, N. A. *Langmuir* **2003**, *19*, 1249.
(29) *)* Patankar, N. A. *Langmuir* **2004**, *20*, 7097.
(30) McHale, G.; Shirtcliffe, N. J.; Newton, M. I. *Langmuir* **2004**, *20*, 10146.
(31) Marmur, A. *Langmuir* **2004**, *20*, 3517.
(32) Krasovitski, B.; Marmur, A. *Langmuir* **2005**, *21*, 3881.
(33) Onda, T.; Shibuichi, S.; Satoh, N.; Tsujii, K. *Langmuir* **1996**, *12*, 2125.
(34) Shibuichi, S.; Onda, T.; Satoh, N.; Tsujii, K. *J. Phys. Chem.* **1996**, *100*, 19512.
(35) Tadanaga, K.; Katata N.; Minami, T. *J. Am. Ceram. Soc.* **1997**, *80*, 1040.
(36) Tadanaga, K.; Katata, N.; Minami, T. *J. Am. Ceram. Soc.* **1997**, *80*, 3213.
(37) Ogawa, K.; Soga, M.; Takada, Y.; Nakayama, I. *Jpn. J. Appl. Phys., Part 2* **1993**, *32*, L614.
(38) Kunugi, Y.; Nonaku, T.; Chong, Y. B.; Watanabe, N. *J. Electroanal. Chem.* **1993**, *353*, 209.
(39) Schakenraad, J. M.; Stokroos, I.; Bartels, H.; Busscher, H. J. *Cells Mater.* **1992**, *2*, 193.
(40) Hozumi, A.; Takai, O. *Thin Solid Films* **1997**, *303*, 222.
(41) Miller, J. D.; Veeramasuneni, S.; Drelich, J.; Yalamanchili, M. R.; Yamauchi, Y. *Polym. Eng. Sci.* **1996**, *36*, 1849.
(42) Ishino, C.; Okumura, K.; Quéré, D. *Europhys. Lett.* **2004**, *68*, 419.
(43) Swain, P. S.; Lipowsky, R. *Langmuir* **1998**, *14*, 6772.
(44) De Coninck, J.; Miracle-Solé, S.; Ruiz, J. *J. Stat. Phys.* **2003**, *111*, 107.
(45) Dupuis, A.; Yeomans, J. M. *Langmuir* **2005**, *21*, 2624.
(46) Porcheron, F.; Monson, P. A. *Langmuir* **2006**, *22*, 1595.
(47) Doshi, D. A.; Shah, P. B.; Singh, S.; Branson, E. D.; Malanoski, A. P.; Watkins, E. B.; Majewski, J.; van Swol, F.; Brinker, C. J. *Langmuir* **2005**, *21*, 7805.

(section 4.2), and then the pillar separation and droplet size (section 4.3). Final remarks and overall conclusions are given in section 5.

2. Simulations

We use a *full* atomistic representation of the water molecules and the surface including long-range electrostatic interactions. The potentials and charges used to describe the water molecules were taken, as previously, from the TIP-3P potential model of Jorgensen et al.[48] For the long-range interactions, a 25 Å cutoff was used, which is larger than one droplet radius. The short-range intermolecular interactions are all of the Lennard-Jones form with a cutoff of 8 Å. For the solid−water interaction (i.e., a solid surface atom interacting with a water oxygen atom), the Lennard-Jones collision diameter σ was kept fixed throughout at 3.0 Å, which is approximately the collision diameter between carbon and water oxygen atoms. The well-depth parameters ϵ are discussed below.

The widely used program DL_POLY was used for the molecular dynamics simulations, which were performed at constant volume and temperature (NVT). (See refs 49−50 for reviews of this code.) The temperature was set to 298 K, which was kept constant by the Berendsen thermostat.[27] All atoms in the solid surface were kept fixed. The simulation time step was set to 1 fs, and the Verlet leapfrog algorithm[52] used for propagation of the position and velocity vectors. Typical lengths of production runs were 500 ps.

The droplet, which comprises ∼1100 water molecules unless otherwise specified (section 4), has a radius of ∼20 Å. The droplet was initially spherical with all molecular orientations set randomly. Initially, the droplet was placed 5 Å above the top atomic layer of the solid surface. After the simulation started, the droplet spontaneously spread over the surface, resulting in a well-defined contact angle. The contact angles are defined as those at the top atomic layer of the pillars and are extracted from the simulations as in earlier publications,[18,19,53] (i.e., by fitting the time-averaged liquid/vapor interface to a circle and obtaining the angle by a simple geometrical calculation). The coordinates for the liquid/vapor interface were calculated over 100 ps and averaged for five runs.

In all simulations, the droplets were placed initially on top of the surface in a random position. Tests showed that the initial position of the droplet did *not* influence the final equilibrium contact angle or the position of the advancing contact line. Formally, the spreading over the heterogeneous surface is a calculation of the advancing contact line. If a different starting configuration were to be selected, such as a monolayer on top of the surface, then possibly a different position of the contact line might be seen, in effect generating the receding contact angle. We have not investigated this issue or any resulting hysteresis.

3. Heterogeneous Surfaces

The heterogeneous solid that we have examined consists of two types of atoms, A and B, with different atom−water potentials in order to simulate a layer with both hydrophobic and hydrophilic regions. The surface is made up of square domains or rectangular stripes of A and B. All surface atom−atom distances are 2 Å.

Table 1. Solid−Liquid Lennard-Jones Parameters Used for the Heterogeneous Surface Studied[a]

	ϵ_A/kcal mol^{-1}	θ_A/deg	ϵ_B/kcal mol^{-1}	θ_B/deg
type I	0.126	101 ± 1	0.040	147 ± 5
type II	0.200	75 ± 3	0.040	147 ± 5

[a] θ_A and θ_B are the contact angles of the water droplet on smooth surfaces of pure A and pure B, respectively.

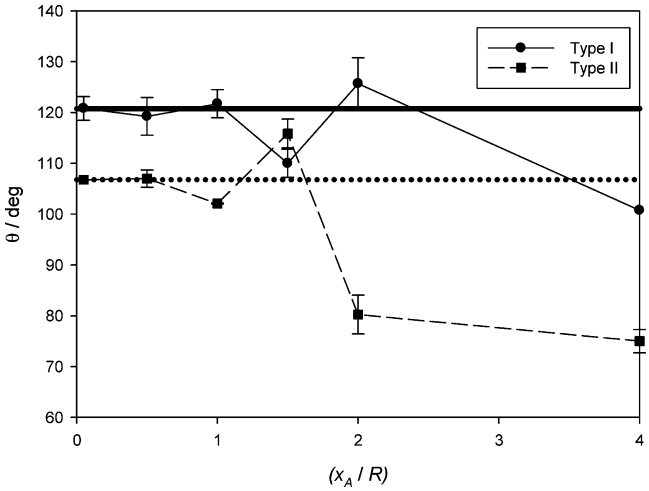

Figure 3. Calculated contact angles for different widths of domains A and B, expressed as the ratio of the domain width to the drop radius (R = 20 Å). The area fractions, f_A and f_B, are kept fixed at 0.5. Circles (●) and squares (■) represent simulated contact angles for type I and type II heterogeneous surfaces, respectively (Table 1). The calculated predictions from the Cassie and Baxter equation are shown for type I and type II surfaces as the solid and dotted straight lines, respectively.

3.1. Nanodroplets and the Domain Size. Simulations of droplets on top of heterogeneous surfaces have been carried out. The fractional areas of the regions of A and B were such that f_A and f_B in eq 1 were both 0.5. The nature of the two regions is altered by changing the solid−water Lennard-Jones potential well depth, ϵ. These parameters are listed in Table 1. Two different types (I and II) of heterogeneous surfaces were examined, with different values of the interaction parameter for the hydrophilic component A (Table 1). Type II is more hydrophilic than type I, for which the surface−water interaction is the same as the carbon−oxygen interaction in the OPLS force field.[54] θ_A and θ_B are the calculated contact angles of the water droplet on smooth surfaces of pure A and pure B, respectively. According to the Cassie equation (eq 3), the equilibrium contact angles for the two types of heterogeneous surfaces with $f_A = f_B = 0.5$ are 107° and 120°, respectively. To investigate the effect of possible variation of the contact angle on the relative sizes of the droplet, the domain widths, x_A and x_B, were varied from 2 to 80 Å. The length of the side of the simulation box was 100−160 Å, thus maintaining a fixed integral number of domains of the desired width in all runs.

The contact angle would be expected[22] to approach the Cassie value when the heterogeneous domains on the surface are sufficiently small relative to the droplet, and this is verified strikingly by the simulated contact angles in Figure 3. When the domains are much larger than the drop radius, the energetically most preferable site for the droplet is the hydrophilic. Now the

(48) Jorgensen, W. L.; Chandrasekhar, J.; Madura, J. D.; Impey, R. W.; Klein, M. L. *J. Chem. Phys.* **1983**, *79*, 926.
(49) Smith, B. W.; Yong, C. W.; Rodger, P. M. *Mol. Simul.* **2002**, *28*, 385.
(50) Todorov, C. I. T.; Smith, W. *Philos. Trans. R. Soc. A* **2004**, *362*, 1835.
(51) Berendsen, H. J. C.; Postma, J. P. M.; Vangunsteren, W. F.; Dinola, A.; Haak, J. R. *J. Chem. Phys.* **1984**, *81*, 3684.
(52) Hockney, D. R. W.; Eastwood, J. W. *Computer Simulations Using Particles*; McGraw-Hill: New York, 1981.
(53) Lundgren, M. Molecular Dynamics Simulations of Wetting. Ph.D. Thesis, University of Bristol, Bristol, U.K., 2003.
(54) Jorgensen, W. L.; Maxwell, D. S.; TiradoRives, J. *J. Am. Chem. Soc.* **1996**, *118*, 11225.

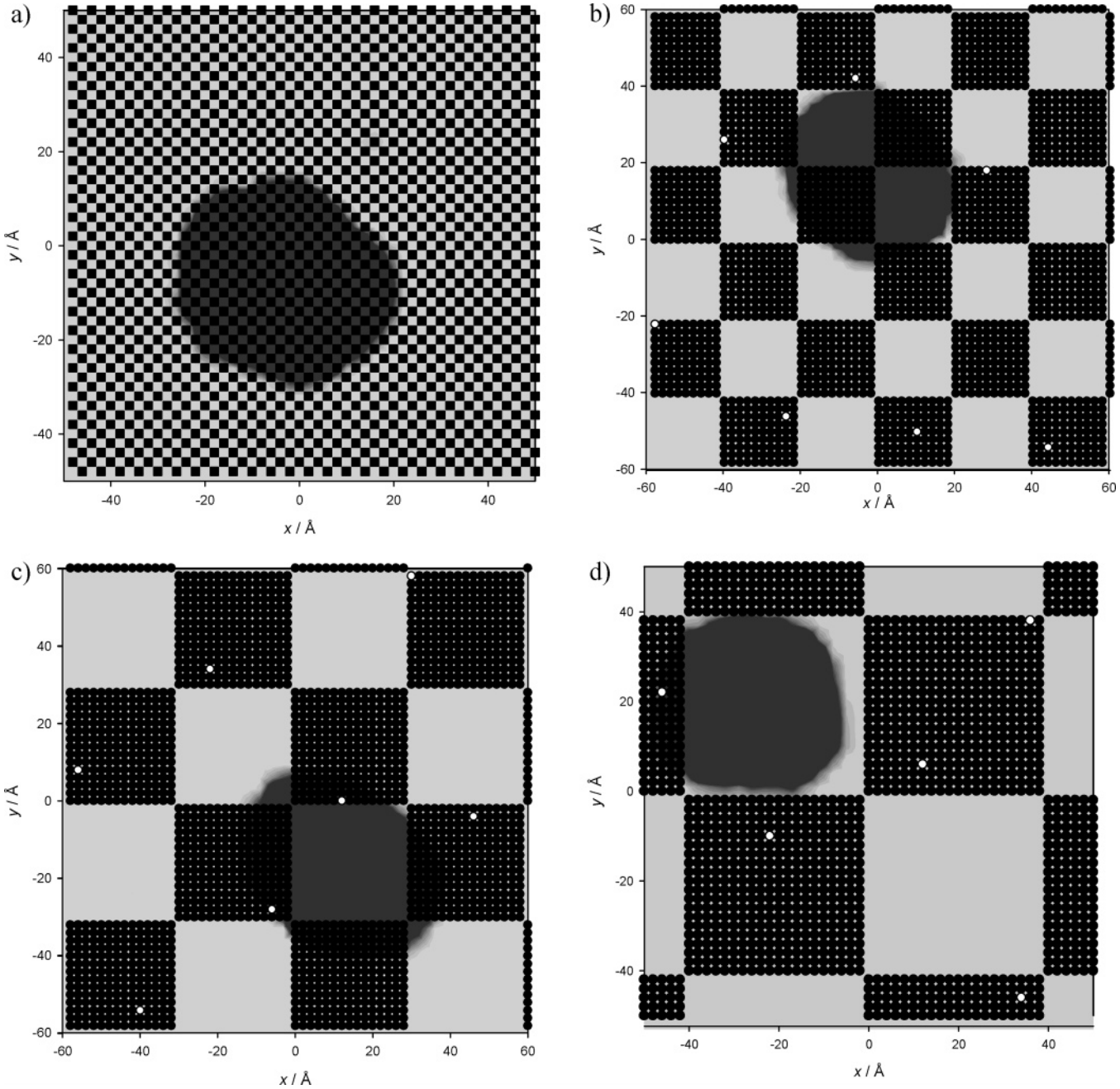

Figure 4. Top views of simulated droplets on heterogeneous surfaces (type I). The dark patches represent the shape of the droplet, averaged over 20 ps. Black dots and light-colored areas represent hydrophobic and hydrophilic domains, respectively. The widths of the domains are 2, 20, 30, and 40 Å for a−d, corresponding to x_A/R values of 0.1, 1, 1.5, and 2, respectively.

droplet wets only the hydrophilic domain, and the contact angle deviates significantly from the Cassie prediction, as can be seen in Figure 3, approaching the value for the pure hydrophilic surface as the domain width, A, x_A, increases.

Figure 4 shows a top view of the hydrophilic heterogeneous (type I) surface. The dark patches represent both the shape of the droplet averaged over 20 ps and the typical position adopted. Figure 3 shows that the contact angle deviates significantly from the prediction from eq 1 for larger heterogeneities, and it is evident in Figure 4 that the droplets are less spherical and more ellipsoidal for larger domains. With the larger domains (especially those in Figure 4b,c), the local contact angle changes from one part of the drop to another as the curvature of the base of the drop varies. Our calculated contact angle plotted in Figure 3 is an average over the entire drop. Such changes in shape are consistent with the numerical energy minimizations of droplets on heterogeneous surfaces by Brandon et al.[22] When the drop diameter is commensurate with the domain size ($x_A/R \approx 1$), the cross sections of the drops are particularly distorted from circular (Figure 4b,c). This leads to larger variations in the average contact angle with domain size, with troughs and peaks (e.g., at $x_A/R = 1.5$), as the drop distorts to increase contact with the more hydrophilic regions. Compare, for example, the different shapes of the drops in Figures 4c ($x_A/R = 1.5$) and 4d ($x_A/R = 2$) and the respective trough and peak in the corresponding plot (type I) in Figure 3. In the largest domain for which values are given in Figure 3 ($x_A/R = 4$), the drop can distort to fit only the hydrophilic part, and the drop maximizes its contact with this favorable region, with an average contact angle close to that for the pure hydrophilic surface.

Simulations have also been carried out to investigate wetting on heterogeneous surfaces composed of stripes of atoms of A

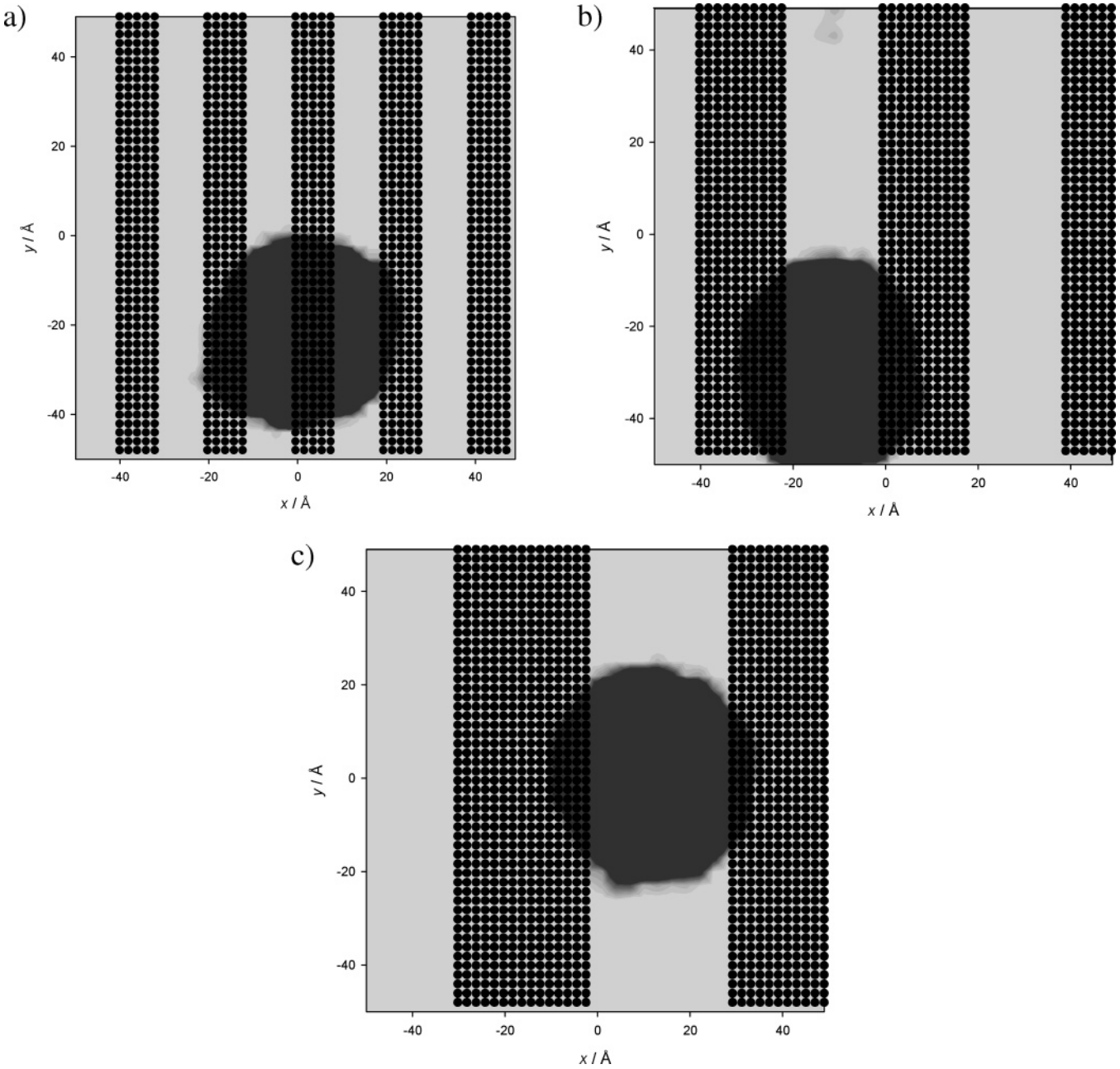

Figure 5. Representative top view of a droplet (dark patch) on top of the striped surface (type I). Black dots and light-colored areas represent the hydrophobic and hydrophilic domains, respectively. The widths of the domains are 10, 20, and 30 Å for a−c, respectively.

Table 2. Lennard-Jones Parameters, ϵ, for the Solid−Liquid Interactions Used in the Study of the Pillar Surface[a]

LJ parameter, ϵ /kcal mol^{-1}	θ/deg
0.300	96 ± 2.3
0.126	125.5 ± 3.4

[a] Contact angles listed for each surface are those calculated for the corresponding atomistic smooth surface.

and B. The same force fields were used (types I and II) as for the square domains (Table 2). The widths of the stripes were varied from 2 to 80 Å. Figure 5 shows that the water droplets at equilibrium are centered over one or more of the hydrophilic stripes and that the shape of the solid/liquid contact line becomes more circular when the widths of the stripes are smaller. The averaged contact angle is a sensitive function of the stripe width, as shown in the plot in Figure 6. The Cassie equation is only a good approximation for the smallest value of the stripe width considered ($x_A \ll R$). The contact angle deviates rapidly from the predicted value with increasing stripe width, rising to a maximum for both types I and II when $x_A \approx R$. For this combination of stripe width and droplet size, the droplet maximizes its contact with the hydrophilic stripe (Figure 3), distorting from its spherical shape to do so. The edges of the droplet overlap with the hydrophobic region, consistent with an increase in the average contact angle. For larger stripe widths (e.g., those in Figure 5c), the distortion of the droplet decreases and the contact angle falls, approaching that of pure water on a homogeneous surface of hydrophilic component A.

3.2. Surface Composition. We have also carried out a short series of simulations on heterogeneous surfaces (type I) composed of square domains in order to investigate the variation of the contact angle with the fractional areas f_A and f_B. Throughout the surfaces, the domains are smaller than the droplet radius. The width, x_B, of the domains of B is varied such that the area fraction, f_B varies from 0 to 1. The side of the simulation box is 100 Å.

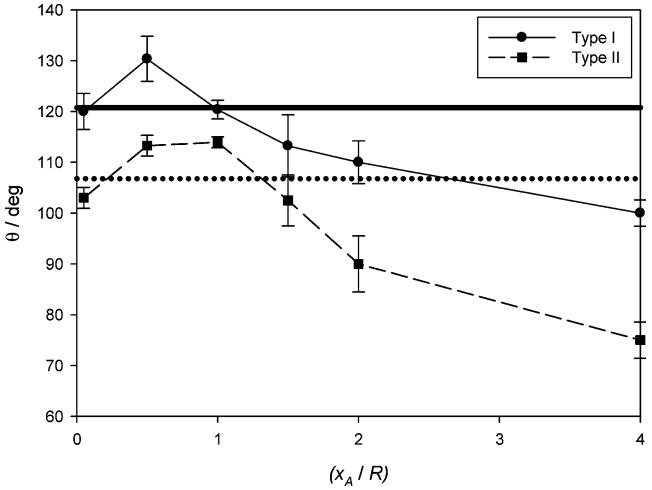

Figure 6. Calculated contact angles for different stripe widths of domains A and B, expressed as the ratio of the stripe width to the drop radius (R = 20 Å). Circles (●) and squares (■) represent simulated contact angles for type I and type II heterogeneous surfaces, respectively. Calculated predictions from the Cassie and Baxter equation are shown for type I and type II surfaces as the solid and dotted straight lines, respectively.

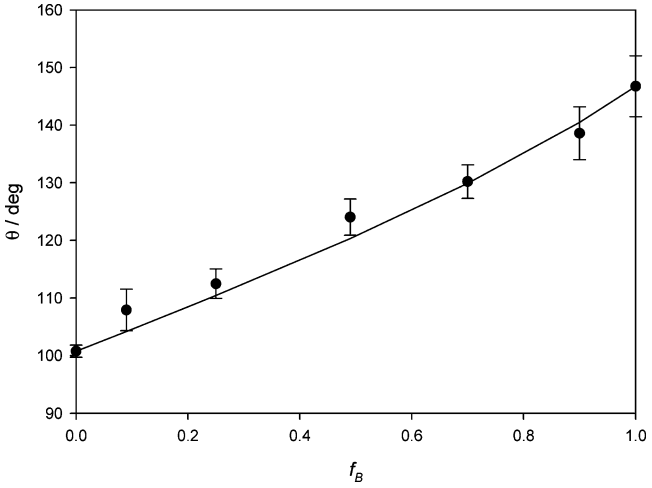

Figure 7. Comparison of the simulated data and calculated (Cassie model, solid line) contact angles for water droplets on heterogeneous surfaces with varying surface concentration of component B.

As plotted in Figure 7, there is an increase in contact angle with increasing concentration of the hydrophobic substrate. The solid line is the contact angle predicted using eq 1. The Cassie model predicts the change in wetting with changes in surface composition rather well.

4. Pillar Surfaces

We turn to consider pillar surfaces. Each surface in our simulations is composed of isotropic cuboidic posts as shown schematically in Figure 8. The atoms are arranged on a cubic lattice with an atom−atom distance of 3 Å. Unlike the graphite surface considered previously,[18] the side and the top of the pillars have the same surface atom density and hence the same wettability here. The cubic simulation box has a side of 100−120 Å. We investigate changes in droplet geometry as a function of pillar height, width, and separation, the effects of changing the interaction potentials between the liquid and the surface, and, briefly, changes with droplet volume.

The hydrophilicity of the pillars is varied by altering the value of the solid−water Lennard-Jones potential well depth, ϵ. The

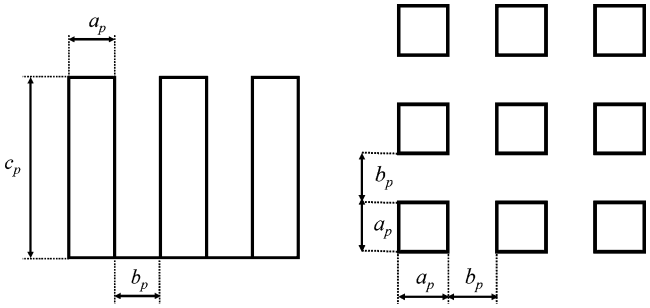

Figure 8. Schematic description of the surface covered with square pillars. The left and right frames show a side and a top view of the surface, respectively. a_p denotes the width, and c_p, the height of the pillar. b_p is the width of the gaps between the pillars.

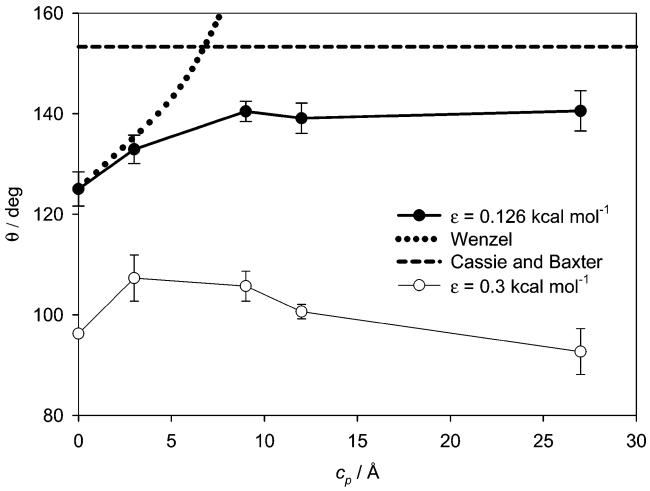

Figure 9. Variation of the calculated contact angle with increasing pillar height.

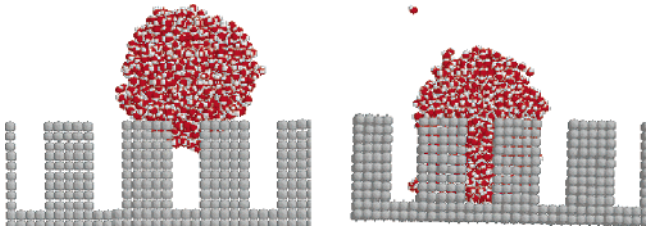

Figure 10. Representative snapshots for droplets on top of a surface composed of pillars with a height of 27 Å. The left and right frames are for the more hydrophobic and hydrophilic surfaces, respectively (Table 2).

two values used are given in Table 2, together with the simulated values of the contact angle for the corresponding smooth surface.

4.1. Pillar Height. Here the pillar width, a_p, and the gap between the pillars, b_p, are kept fixed at 15 and 9 Å respectively. The height, c_p, varied from 3 to 27 Å. Figure 9 shows calculated contact angles for water droplets of 20 Å radius for the two potentials listed in Table 2. For the smallest pillar height (one atom high), the gaps between the pillars are wetted, and the contact angles are larger than for the smooth surface, in qualitative agreement with Wenzel's equation (Figure 9), as shown, for example, by the curved dotted line in Figure 9 for the more hydrophobic case.

Considering first the more hydrophobic surface, the contact angle continues to increase until c_p reaches approximately 9 Å. Whereas this is still in qualitative agreement with the argument of Wenzel (eq 2), quantitative agreement is poor. One reason is evident from Figure 10. When c_p is 9 Å, the droplet does not penetrate to the bottom of the gaps, and the edge of the droplet

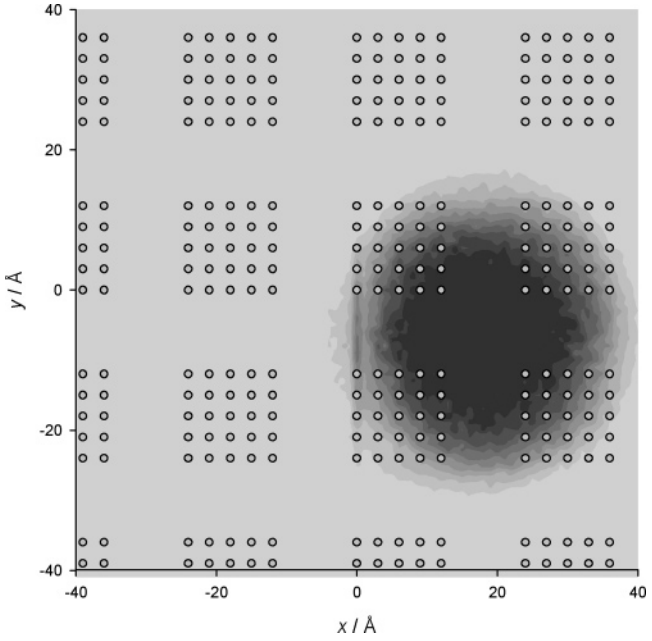

Figure 11. Water droplet on top of the hydrophobic pillar surface ($c_p = 12$ Å). The dark region indicates the position of the droplet, and the open circles represent the position of the solid surface atoms for the pillars. The droplet geometry shown has been averaged over 20 ps.

is pinned to the top corners of the pillars. The treatment of Wenzel does not take into account the effect of sharp corners where the density of surface atoms is particular high. The trapped droplet is clearly influenced by the corners of the cuboidic posts because limited penetration into the gaps is observed. Further increase of the pillar height above 9 Å results in a crossover to the Cassie and Baxter regime. The droplet is located at the top of the pillars, and the penetration into the gaps remains restricted. The contact angle is now independent of further increase of the pillar height, in qualitative agreement with the Cassie and Baxter model.[25] Quantitatively, the use of eq 3 leads to an overestimate of the contact angle because the Cassie and Baxter approximation neglects the (limited) penetration into the gaps.

Also evident in Figure 9 is the slight decrease in the contact angle with the height of the posts in the more hydrophilic case. The hydrophilic nature of the solid surface results in the droplet penetrating the gaps even when the pillar height is increased to a very high value. This causes a volume loss in the main body of the drop located above the pillars. Because the contact angle is measured at the top layer of the pillars, this changes the drop radius/pillar width ratio, and there is a decrease in contact angle as can also be seen in Figure 10.

The contact line is located in all of these simulations close to the edge of four pillars as seen in Figure 11. It is worth noting that the contact line will be quite different if the width of the pillar is changed as discussed in the next section.

4.2. Pillar Width. To investigate further the importance of the position of the contact line, the width of the cuboidic pillars was varied from 3 to 30 Å. The height of the pillar, c_p, is fixed at 15 Å, and the gap between the pillars, b_p, 9 Å. For this geometry, when the Lennard-Jones well depth ϵ is 0.126 kcal mol^{-1}, no water molecules penetrate the hollows, and the system is in the Cassie and Baxter regime.

For extremely thin pillars of width of 3 Å, complete repulsion of the droplet from the surface is observed. This is due to the very low fraction of the liquid/solid interface (∼1%), and in agreement with the Cassie and Baxter equation (eq 3), this results

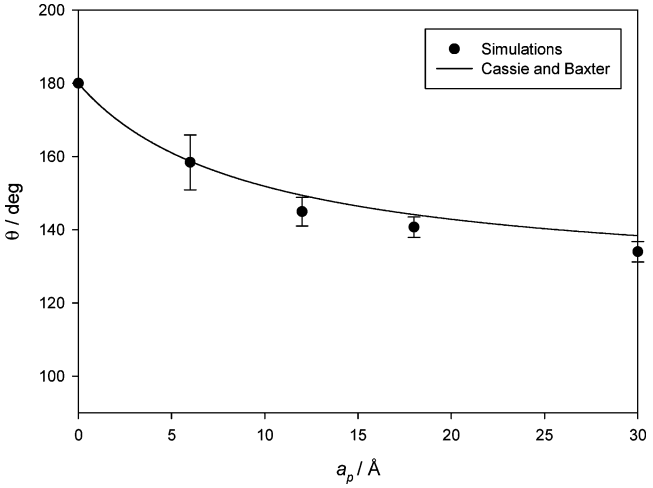

Figure 12. Simulated contact angle on surfaces with increasing pillar width, a_p, compared with the predictions of the Cassie and Baxter equation. The droplet radius is 20 Å.

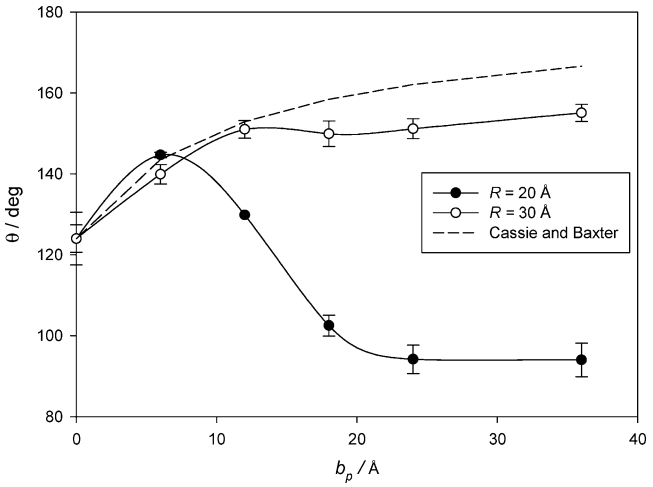

Figure 13. Variation of the contact angle with the gap between the pillars for the more hydrophobic surface and droplet radii of 20 and 30 Å. The pore size, b_p, is defined in Figure 8. The dashed line is the contact angle predicted using the Cassie and Baxter equation (eq 3).

in superhydrophobicity and a contact angle of 180°. As shown in Figure 12, the spreading increases when the pillars widen and f increases. For wider pillars, the surface area of the top of the pillars is larger, which enhances wetting, and when the pillar width is very much greater than the diameter of the droplet and the gaps between the pillars, the droplet takes up a contact angle similar to that for a perfectly smooth surface. In all cases, no penetration into the hollows is seen.

4.3 Gap Size. Changing the distance between the pillars changes the ability of the water droplet to penetrate the surface. The model surface was again composed of a flat lattice surface decorated with cubiodic posts. The pillar height and width were kept fixed at 15 and 12 Å, respectively, and the distance between each pillar varied from 6 to 36 Å. In addition, to see the effects of increasing droplet size, simulations of a droplet with a radius of 30 Å, containing 3818 water molecules, were carried out, as well as carrying out simulations, as earlier, for a droplet radius of 20 Å.

The simulated contact angles for both droplets and gap sizes up to 10 Å are in good agreement with the Cassie and Baxter prediction as f increases (Figure 13). For a 20 Å droplet, this comes to an abrupt halt when the droplet starts to penetrate into the gaps between the pillars and the contact angle decreases.

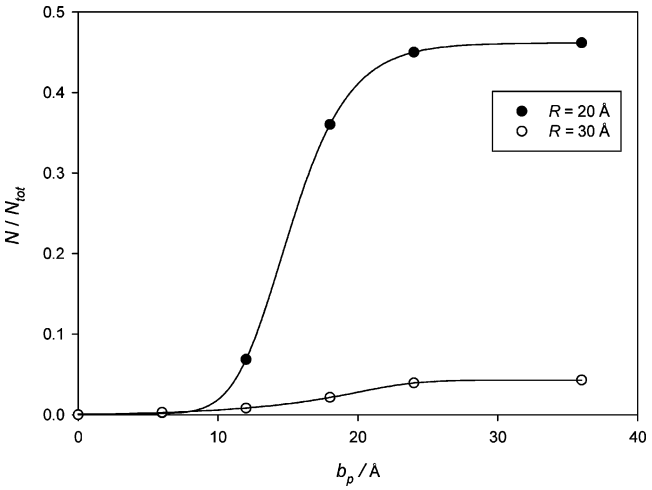

Figure 14. Number fraction of water molecules, N/N_{tot}, that have penetrated into the gaps for different droplet sizes, *R*. The gap width (pillar separation), b_p, is defined in Figure 8.

The degree of penetration varies with the ratio of the gap width and the drop radius. The dependence of the equilibrium contact angle on gap size for the 30 Å radius drop (Figure 13) is quite different from that of the smaller droplet for pillar separations > 10 Å. The larger drop remains on top of one pillar, and we remain essentially in the Cassie and Baxter regime even for large gaps between the pillars, even though the contact angle is effectively constant with gap size. This is reflecting the behavior at the sharp corners of the pillar, as noted above.

The amount of water that penetrates into the gap was analyzed for each surface by calculating the average number of water molecules located below the top plane of the pillars, and the results are plotted as a function of the gap between the pillars in Figure 14. For pillar surfaces with small gaps, no penetration of water molecules can be seen. The system is fully in the Cassie and Baxter regime, and the contact angle is close to that of the flat heterogeneous surface. When the gap size becomes sufficiently large, the small water droplet partially penetrates the hollows. The larger drops do not penetrate the gaps between the pillars at all, even when the droplet radius is comparable to the gap size, and Figure 14 shows that there is only a small increase in the penetration of the water molecules for large gap sizes. As discussed above, for wide hollows the droplet is pinned to the top of the pillars and did not penetrate the gaps. The droplet may eventually be able to move away from the top of the post and down to the hollows, but this was never observed during any simulation run. Enhanced stability of the larger droplet is consistent with nonpenetration when the drop size increases. Less evaporation was also seen from the larger drops, which also indicates enhanced stability for the larger droplet with smaller surface curvature in qualitative agreement with the Kelvin equation.

5. Conclusions

The simulations of water droplets presented in this article have shown the importance of the detailed topography and composition of the solid surface and clearly indicate situations where the contact behavior is not well described by the Wenzel, Cassie, or Cassie and Baxter equations.

When surfaces are planar, consisting of domains of different hydrophobicity and size, for small droplets, the relative sizes of the droplet and the domain play an important role. If the surface domains are sufficiently small, then the droplet effectively wets a large number of domains, and the Cassie equation accurately describes the relation between the contact angles and the surface composition. If the relative size of the domains is larger, then this equation fails, and the wetting is largely constrained by the surface geometry. The water droplet favors the hydrophilic regions of the surface, and there may be significant elongation or contraction of the droplet in certain directions, particularly when the drop and the domain size are commensurate, so as to maximize this interaction.

For pillar surfaces, the treatment of Wenzel assumes that the liquid wets all of the surface area. In contrast, that of Cassie and Baxter suggests that rough wetting is associated with quite different atomistic behavior; the liquid does not penetrate the hollows of the rough surface, and thus the droplet feels a heterogeneous surface composed of sections of solid and sections of air or vacuum. This results in increased hydrophobicity with increasing roughness and an increase in the contact angle. The simulations indicate the Wenzel and the Cassie and Baxter regimes occur for different heights of the cuboidic pillars. Wetting of small pillars is accompanied by penetration into the gaps between the pillars (the Wenzel regime). When the pillar height is increased, the droplet remains on top of the pillars (the Cassie and Baxter regime). The contact angles are largely independent for pillar heights > 15 Å. Quantitatively agreement between the simulated contact angles and those predicted by the Wenzel and the Cassie and Baxter equations is generally rather poor. These equations do not take into account the surface geometry and the effect of sharp corners on the surface where the density of adsorption sites is particularly high.

To conclude, molecular dynamics simulations reveal a rich variety of behavior at the atomic level associated with nanowetting phenomena. With simulations of this type, we can now begin to tackle many related questions such as the effects of surfactants or of particular surface defects, the details of the dynamic processes associated with the spreading of the droplets, and, as methodology advances and available computer time increases, the relations between nanoscale and macroscopic behavior.

Acknowledgment. We are grateful to EPSRC for financial support and Neil George at Syngenta for additional support and useful discussions. Computational facilities were provided by EPSRC and HEFCE JREI awards (the Mott2 machine at Rutherford and the Dirac machine at Bristol).

LA060712O